



# Study on deformation characteristics of tunnels excavated in jointed rock masses through field testing and numerical methods

Dongyang Yuan<sup>1</sup> · Changdi He<sup>1,2</sup> · Fei Peng<sup>1</sup> · Weikang Zhang<sup>1</sup> · Haozheng Wang<sup>1</sup> · Yongyong Yang<sup>1</sup> · Yongjun Liu<sup>3</sup> · Qiang Wang<sup>1</sup>

Received: 16 December 2021 / Accepted: 11 April 2022 / Published online: 24 April 2022  
© Saudi Society for Geosciences 2022

## Abstract

Jointed rock masses contain complexly distributed fractures that have significant impacts on the mechanical behavior of the surrounding rock, especially during the tunneling process. In this paper, a field test was carried out to record the vertical displacement and deformation of the constructing tunnel passing through jointed rock masses. To further investigate the deformation characteristics of tunnels excavated in jointed rock masses, numerical simulations utilizing discrete element methods (DEM) were conducted. Numerical models simulated different sizes and shapes of blocks in jointed rock masses. The results show that during the process of tunnel excavation, the vertical displacement of surrounding rock undergoes the rapid growth phase and the gradual stabilization phase, and the time interval of these two stages is different due to the different depths of the tunnel. In the same monitoring section, the closer to the vault of the tunnel, the larger the vertical displacement of the monitoring point. The displacement value of the section closer to the tunnel face is larger than that far away from the tunnel face, while the tunnel section in shallower buried depth performs relatively larger liner deformation. For the same size of blocks, jointed rock masses formed by tetrahedral blocks perform relatively larger vertical displacement of surrounding rock, deformation of the tunnel, and positive and negative moments of liner structures than those formed by cubic or polyhedral blocks.

**Keywords** Tunnel · Jointed rock masses · Displacement · Deformation

## Introduction

Jointed rock masses are widespread in the natural world, and they influence the long-term deformation and stability of engineering structures. In recent decades, with the

continuous progress of engineering technology, the construction of large mountain highway tunnels, hydraulic tunnels, and mine tunnels has made massive breakthroughs. However, the existence of complex structural planes in rock masses might easily cause safety accidents, such as structural instability and collapse owing to the lack of integrity, overall strength, and self-stabilization capability of surrounding rock when tunnels pass through the well-developed jointed and fractured rock masses (Yang et al. 2019b).

Joints have significant impacts on rock masses under static and dynamic conditions (Li et al. 2019b; Wang et al., 2022). Different distributions and features of joints such as the joint thickness (Yang et al., 2019a), joint plane angle (Zhou et al., 2019), and lamination properties (Shi & Mishra, 2021) have various effects on the properties of rock masses since rock joints have a nonlinear mechanical pattern during loading while a nearly linear pattern during unloading process in the tensile stress–strain curves (Han et al., 2020). Joint factor, a weakness coefficient, can be used to describe the effect of joints in rock masses (Singh et al. 2002). Pan

---

Responsible Editor: Zeynal Abiddin Erguler

✉ Changdi He  
chardyhe@outlook.com

✉ Yongjun Liu  
328885389@qq.com

<sup>1</sup> Key Laboratory of Road and Bridge Detection and Maintenance Technology of Zhejiang Province, Zhejiang Scientific Research Institute of Transport, Hangzhou, China

<sup>2</sup> Department of Mining Engineering, University of Utah, Salt Lake City, USA

<sup>3</sup> Huzhou Port & Shipping Management Center, Huzhou, China

et al., (2021) presented that the inter-granular tensile cracks dominate the rock fracturing under blast loadings through a hybrid LS-DYNA and UDEC grain-based discrete element method (UDEC-GBM). Besides, under the blasting condition, there is a remarkable stress concentration at the joints, which might promote the crack initiation and propagation (Yang et al., 2018).

Joints distributed in surrounding rock bring great difficulties and risks to the tunnel excavation. There are many influencing factors of jointed rock mass on failure mode and displacement characteristics of the tunnel, such as the joint size (Panthee et al., 2016), joint spacing (Jiang et al., 2018); W. Zhang et al., 2020); Qu et al., 2021), joint angle (Do & Wu, 2020; R. Zhang et al., 2019; Gao et al., 2017), lateral pressure coefficient (Jia & Tang, 2008), pre-existing fractures (Lei et al., 2017; Z. Wang et al., 2021), and joint thickness (Li et al., 2019a). Different types of joints in surrounding rock will form different fractures. Large fractures enable to keep stable after excavation; however, with the increase of small fractures, the EDZ (Excavation Damaged Zone) is mainly generated by the coalescence of small fractures near the tunnel boundary. The surrounding rock deformation modes can be divided into three types, i.e., shear deformation pattern, mixed deformation pattern, and normal deformation pattern (Li et al., 2019a). Related scholars have summarized the failure modes of tunnels in jointed rock masses. The process of intact or jointed rock fragmentation can be divided into three stages, i.e., the loading stage, unloading stage, and residual leaping broken stage, and the presence of the joints will make the unloading stage in advance. Besides, the failure patterns for jointed rock damage can be classified into four types: joint-prevent failure mode, joint-propagation failure mode, joint-tendency failure mode, and joint-initiation failure mode (Jiang et al., 2018).

At present, the methods to study the failure mechanism of tunnel excavation in jointed rock mass mainly include field tests, model tests, theoretical analysis, and numerical simulation (Li et al., 2019a; Wang et al., 2020). DFN-DEM,

UDEC-DFN, PFC (Shi et al., 2022), and finite element analysis (Khan et al., 2021) were widely used in analyzing the tunnel excavation response in jointed rock masses, and discrete fracture networks (DFNs) can be generated using MoFrac (Wang & Cai, 2020), rock failure process analysis (RFPA) (Jia & Tang, 2008), or Fish code (He et al., 2018). Besides, multiple methods have also been developed. For example, tunnel seismic prediction (TSP) and discrete element method (DEM) were combined to analyze the jointed rock mass stability (Fan et al., 2021). Terrestrial laser scanner (TLS) geological mapping was proposed to automatically generate DFNs (Cacciari & Futai, 2017); using the hybrid finite-discrete element method (FEMDEM) to capture the deformation of intact rocks, the interaction of matrix blocks, the displacement of natural fractures, and the propagation of new cracks (Lei et al., 2017). Moreover, to overcome the difficulties of insufficient joint specimens with identical natural morphologies for experiments, three-dimensional (3D) optical scanning and 3D rigid engraving have been proposed (Jiang et al., 2020).

In this paper, we combined field testing and numerical simulation methods to analyze the deformation characteristics of tunnels excavated in jointed rock systems with different sizes and shapes of blocks in jointed rock masses. The research results of this paper are aimed to help analyze the characteristics of tunnel construction in the fractured surrounding rock so as to better control the deformation and failure of the tunnel.

## Engineering background

A shallow buried freeway tunnel located in China is constructed in weathered rock with weak mechanical strength due to the well-developed joints and cracks. Figure 1 illustrates the topographic and geological section map. The entrance and exit sections of the tunnel are curved. Besides, the tunnel passes through a small ridge with steep slopes.

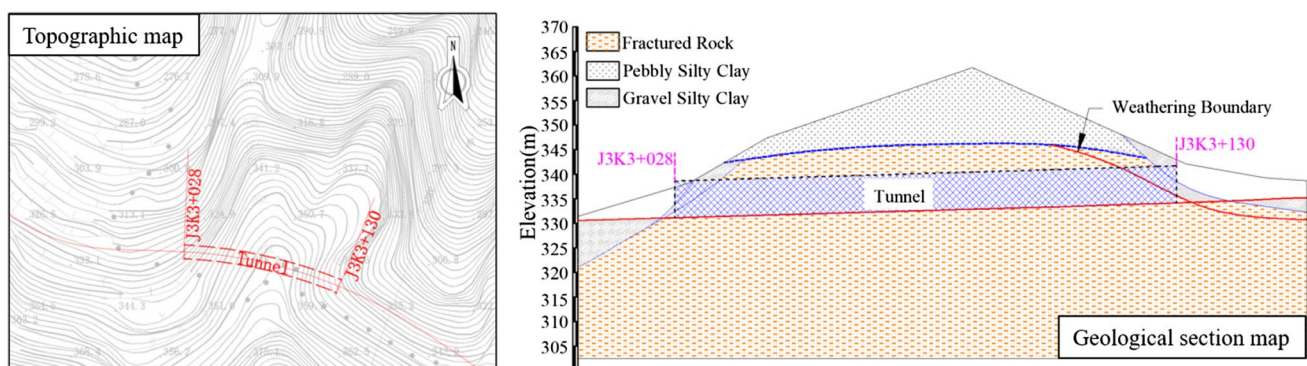


**Fig. 1** Topographic map and geological section of the constructing tunnel

The geological section of the construction spot demonstrates that the maximum buried depth of the tunnel is about 20 m, and the length of the tunnel is 102 m. The tunnel is constructed in fractured rock whose joints and fissures are densely developed. The surface lithology of the tunnel exit section is similar to that of the tunnel entrance section, with different thicknesses ranging from 0 to 3.1 m.

The failures of the constructing tunnel include cavity collapse, arch collapse, and collapse of the tunnel face. The presence of joint structures makes it difficult to form the self-stability of the surrounding rock during excavation owing to the loose status of the fractured rock. Hence, under the disturbance of the construction loading, it is easy to occur tunnel deformation or even collapse. After the arch collapse, block masses will fall on the steel mesh frame of the liner and cause deformation of the steel mesh frame, thus will seriously affect the quality of the liner. When the tunnel is excavated to a certain distance, the loose surrounding rock ahead of the tunnel face gradually becomes unstable and begins to collapse into the tunnel.

Therefore, it is of great significance to explore the behaviors of the tunnels excavated in the jointed surrounding rock under different conditions. Analyzing the deformation characteristics of the tunnel structure is beneficial to predict the unstable and hazardous areas in advance and to take control measures timely.

## Study on ground displacement and tunnel deformation

### Field monitoring of ground displacement

In this study, the overall process of monitoring the ground displacement was carried out before the tunnel excavation by embedding multi-point displacement sensors (BGK-4450) from the ground surface. Once displacement or deformation occurs, the monitoring rod will be dragged by the anchor head of the sensor, and the monitoring rod will then pull the tie rod installed in the

transition tube, to produce displacement. The displacement of the tie rod is transmitted to the internal vibrating wire, which is transformed into the change of the vibrating wire stress, thereby changing the vibration frequency of the vibrating wire. The frequency signal is transmitted to the recording device through the cable, and the displacement or deformation of the measured structure can be monitored through transformation. Meanwhile, by controlling the length of the monitoring rod, the displacement or deformation of the structure at different positions can be recorded.

Figure 2 is the layout of monitoring sections and points in the field testing. There are three monitoring sections laid out in the field test, and each monitoring section was buried with three measuring points, all of which were located directly above the central axis of the tunnel. The mark of roadway stake of section No. 1, No. 2, and No. 3 is J3K0+049, J3K0+054, and J3K0+061, respectively. The distance between the three monitoring points of each monitoring section and the tunnel vault is 1 m, 2 m, and 3 m. Vertical deformation of three monitoring sections (No. 1, No. 2, and No. 3) mentioned above was recorded in the field testing. Reflectors were installed on the surface of the tunnel liner, and the total station was employed to measure the displacement of reflectors through the non-contact test. When the tunnel was excavated to distances between three sections (from  $0.2D$  to  $4D$ , interval  $0.2D$ ), the deformation data would be monitored. The detailed information regarding the buried depth of the three test sections is shown in Table 1. The installation procedure of multi-point displacement sensors can be divided into the following steps:

- (1) Drilling testing holes: using the rig to drill holes with a diameter of 12 cm at the correct depth.
- (2) Preparing and setting rod: the corresponding length of the rod and the anchor head were assembled according to the pre-set buried depth. The safety rope was bound

**Fig. 2** Layout of monitoring sections and points in the field testing

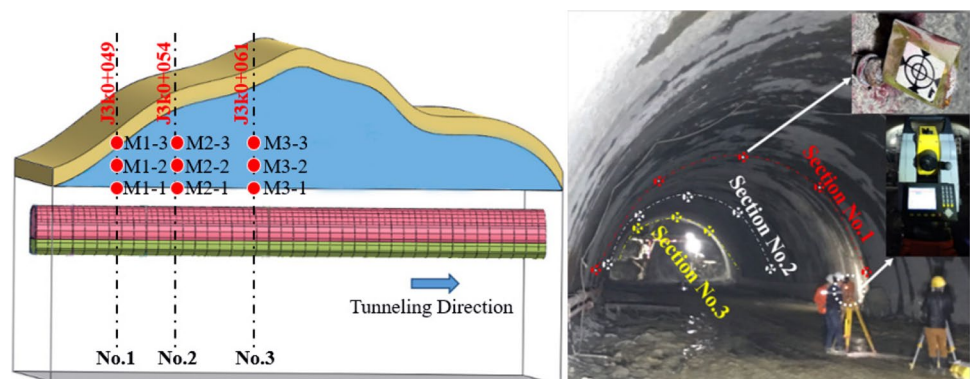


**Table 1** Embedment depth information of multi-point displacement sensors

Sections	Stake	Tunnel depth (unit: m)	Monitoring points	Monitoring point depth (unit: m)	Distance from the monitoring point to the vault (unit: m)
No. 1	J3K0+049	7	M1-1	6	1
			M1-2	5	2
			M1-3	4	3
No. 2	J3K0+054	9	M2-1	8	1
			M2-2	7	2
			M2-3	6	3
No. 3	J3K0+061	14	M3-1	13	1
			M3-2	12	2
			M3-3	11	3

at the position of the anchor head to accurately control the buried depth.

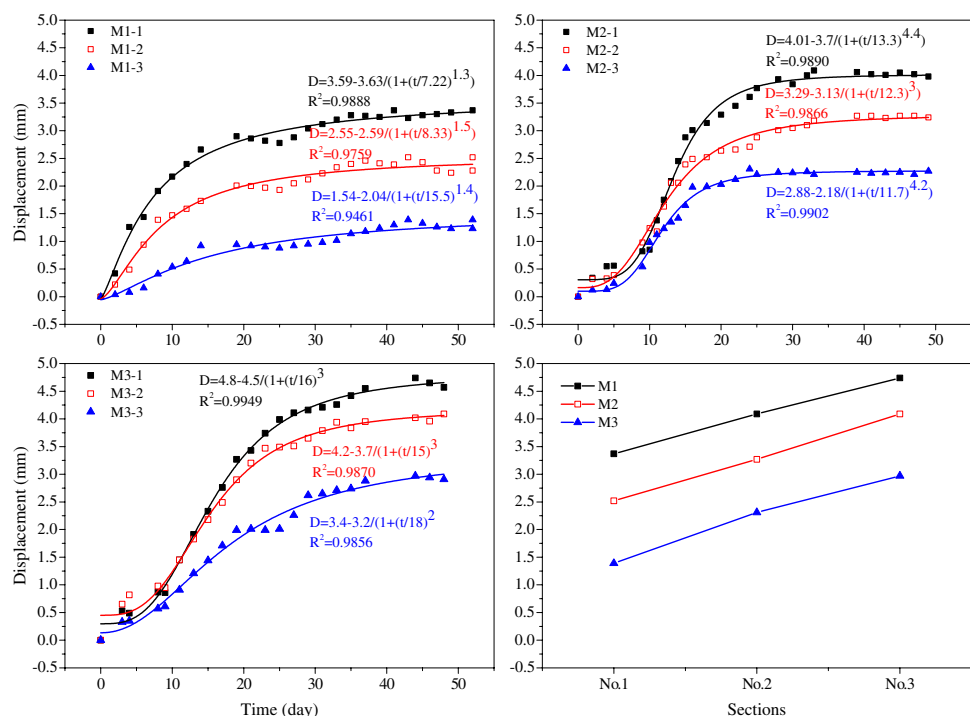
- (3) Placing and connecting sensors: appropriate amount of concrete was poured so that the anchor head would be tightly anchored to the surrounding rock. A certain amount of concrete should be filled into the testing hole to the buried depth of the next measuring point after the installation of the former testing rod was completed. To facilitate the subsequent installation of displacement sensors, the tips of three measuring rods should be located in the same horizontal plane. The displacement sensor was connected to the top of the rod and fixed on the dedicated installation base, and then, the protection tube and the sensor protective cover were installed in turn.
- (4) Collecting and processing data.

### Analysis of the field testing data

All field testing data are statistically analyzed, and vertical ground displacement curves are shown in Fig. 3. According to the time-displacement curves, for the same monitoring section, the displacement value increases with the increase of the depth of the measuring point as the stress of surrounding rock is mainly caused by the dead weight of rock mass.

With the increase of time, the displacement of surrounding rock at different depths increases gradually. The displacement of the surrounding rock undergoes two phases, i.e., rapid growth phase and gradual stabilization phase. The time interval of these two stages is different due to the different depths of the tunnel and the monitoring point. In the same monitoring section, the closer to the top of the tunnel,

**Fig. 3** Vertical displacement at different sections of tunnel



the larger the displacement of surrounding rock mass. The main reason might be that the vertical displacement of surrounding rock near the tunnel face is also affected by the backside excavated zone. For example, when the excavation distance is small, the excavation disturbance range is limited, and thus, the vertical displacement is relatively smaller. However, after tunneling for a long distance, the region backside the excavated zone will influence the vertical displacement near the tunnel face. On the contrary, the displacement of the surrounding rock far away from the top of the tunnel is relatively small. For different monitoring sections, at the same length of the tunnel vault, the displacement of the measuring points decreases gradually with the increase of the buried depth of the overlying rock masses.

Figure 4 is the vertical deformation of the tunnel when the excavation comes to certain distances. With the advance in tunnel excavation, the vertical deformation of the tunnel increases gradually, but the deformation rate decreases gradually, and finally reaches a stable state. The final stable deformation value of section No. 1 is relatively greater than sections No. 2 and No. 3 which are close to the tunnel face. The reason may be that the buried depth of section No. 1 is shallower, and the self-stability ability of the surrounding rock after excavation is weaker than that of the tunnel section with a large buried depth.

The deformation process of the surrounding rock is complicated and incorporates not only rheological deformation but also elastic–plastic deformation and discontinuous deformation of rock. Theoretically, if the tunnel excavation is completed in an instant and the strength of the surrounding rock does not change in the process of elastic–plastic deformation, then the plastic zone and elastic zone will gradually form from the outside to the inside after the tunnel excavation. When the above conditions are met, the time

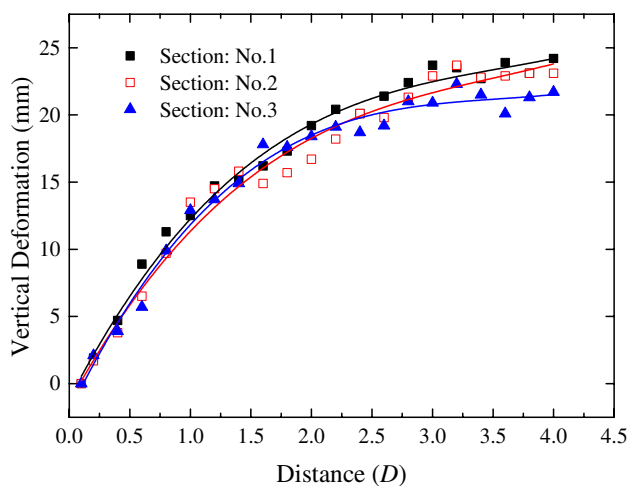


**Fig. 4** Vertical deformation of the tunnel when the excavation comes to certain distances

required for the formation of the plastic zone and the elastic zone is relatively short, and it can be approximated that the elastoplastic deformation of the surrounding rock is completed instantly. However, in fact, the tunnel excavation is not completed in an instant, and the surrounding rock stress is constantly changing. Therefore, the elastoplastic deformation of the surrounding rock cannot be completed instantly but develops gradually with the change in distance, and the length of the influence time is determined by the tunneling speed.

Through the analysis of the field test data, we qualitatively understand the deformation characteristics of tunnels excavated in jointed rock masses. However, we can hardly judge the influence of jointed rock masses on the tunnel deformation characteristics during the excavation. Hence, in the following section, we will use the discrete element method to study the influence of different jointed rock masses with various sizes and shapes of blocks in fractured rock masses on tunnel deformation characteristics during the excavation process.

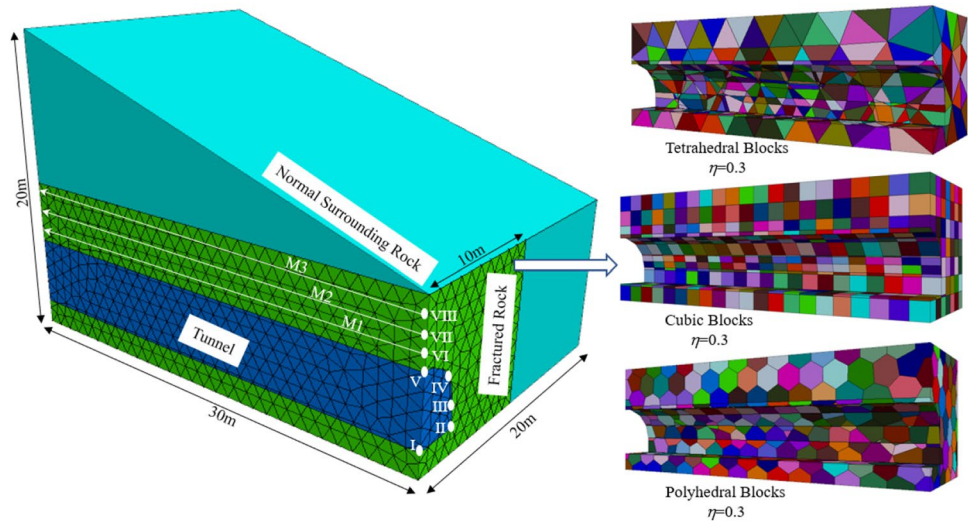
## Numerical models establishment and parameters selection

### Numerical models

In this section, discrete element software (3DEC) is employed to simulate the deformation features of the tunnel excavated in jointed rock masses. Figure 5 illustrates the numerical simulation model built up in this paper, and its length and width are 30 m and 20 m; the height goes from 10 to 20 m, which enables it to simulate different buried depths of the tunnel. To save computational resources, the numerical model is divided into three groups, i.e., fractured rock, normal surrounding rock, and tunnel. The tunnel is built in the fractured rock region, and liners are set after every 3-m-tunneling along the direction of increasing buried depth. The monitoring sections and related measuring points in the surrounding rock can be conducted to record the ground movement of the upper surrounding rock and tunnel deformation characteristics. Along the tunneling direction, several monitoring points are set on M1, M2, and M3 at 1 m intervals above the tunnel vault to monitor the vertical displacement of surrounding rock. Figure 5 are selected numerical models with different sizes and shapes of blocks in fractured rock ( $\eta=0.3$ ). Three shapes of blocks are discussed in this paper, i.e., tetrahedral, cubic, and polyhedral blocks.  $\eta$  is the number of blocks per unit volume of fractured rock, larger  $\eta$  represents more blocks in fractured rock, and the value of  $\eta$  0.3, 1, 2, 4, 9, and 14 are discussed in this paper, respectively.

The Mohr–Coulomb joint model is adopted for numerical simulation, which provides the linear expression of joint

**Fig. 5** Numerical models and monitoring points set in simulations



stiffness and yield limit based on rock joint parameters such as elastic stiffness, friction, cohesion, tensile strength, and dilation characteristics. The displacement-weakening of joints is simulated through the loss of cohesion and tensile strength at the beginning of shear or tensile failure (Itasca, 2020).

The peak shear stress is given by  $S_F^{peak} = c + \sigma_n \tan \phi$ , where  $c$  is the cohesion,  $\sigma_n$  is the normal stress, and  $\phi$  is the friction angle. The residual strength can be expressed by  $S_F^{res} = c_{res} + \sigma_n \tan \phi_{res}$ , where  $c_{res}$  is the residual cohesion, and  $\phi_{res}$  is the residual friction angle.

Table 2 is the mechanical parameters of the surrounding rock and supporting structure, the normal rock and liner adopt the elastic model; the joints employ the Mohr–Coulomb joint model.

**Analysis of numerical results**

**Verification between the field test and numerical simulation**

Figure 6 is the vertical displacement of the surrounding rock (cubic blocks) at different sections of the tunnel. The excavation progress

has been normalized in the range of 0 to 1. Similarly, with the progress of tunnel excavation, the vertical displacement values of monitoring points at three monitoring sections gradually increase and eventually reach a stable value. The final vertical displacement values of the tunnel section far from the tunnel face are relatively large (section No. 1). These rules are consistent with the field test results, indicating that the numerical simulation in this paper has provided a relatively reliable reference for subsequent research. Meanwhile, with the increase of the value of  $\eta$ , the vertical displacement of surrounding rock increases.

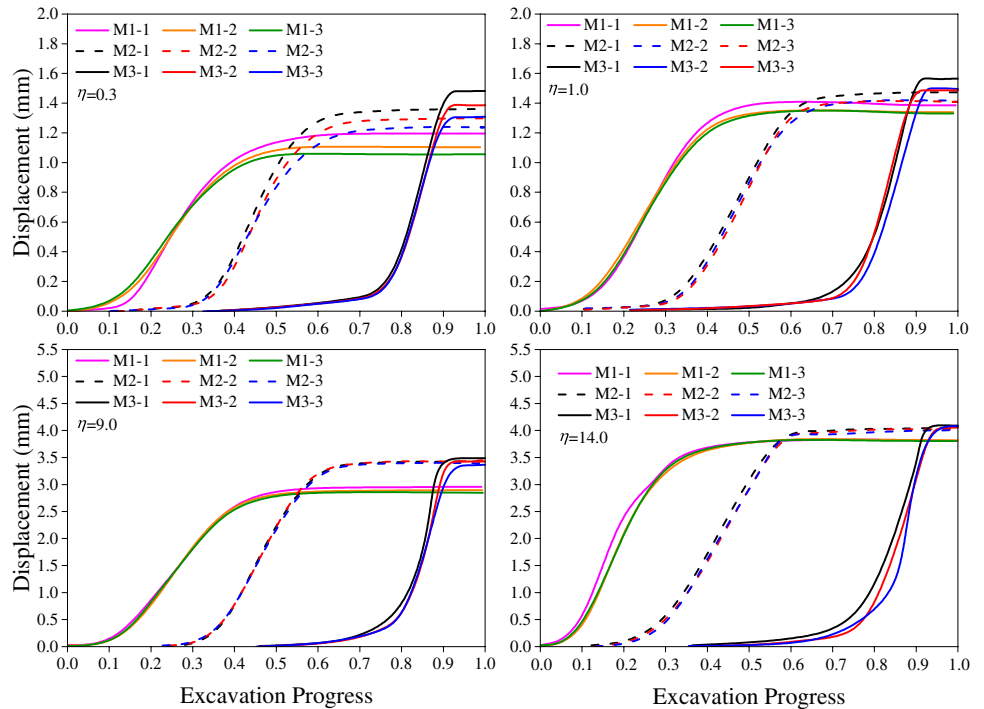
**Maximum displacement of surrounding rock**

Figure 7 is the maximum displacement of surrounding rock with different sizes and shapes of blocks. In the fractured rock with tetrahedral blocks, the maximum displacement of the strata varies greater at each monitoring point along the excavation direction of the tunnel than in other two shapes of blocks, especially in the cases of a large value of  $\eta$ . Besides, the change of maximum displacement along the M1, M2, and M3 are similar; i.e., the variation of maximum displacement is far more fluctuant induced by the increase

**Table 2** Mechanical parameters of the surrounding rock and supporting structure

Items	Material properties	
Rock	Density: $\rho = 2200 \text{ kg/m}^3$ ; Poisson's ratio: $\mu = 0.3$	Young's modulus: $E = 3 \text{ GPa}$
Joints	Joint normal stiffness: $k_n = 0.8 \text{ GPa}$ ; Joint friction angle: $\phi = 22^\circ$	Joint shear stiffness: $k_s = 0.1 \text{ GPa}$
Liner	<b>Liner properties:</b> Young's modulus: 20 GPa Poisson's ratio: 0.15 Thickness: 0.2 m	<b>Liner-rock contact:</b> Cohesion: 15 GPa Friction angle: $50^\circ$ Normal stiffness: 60 GN/m Shear stiffness: 40 GN/m Tensile strength: 8 GPa

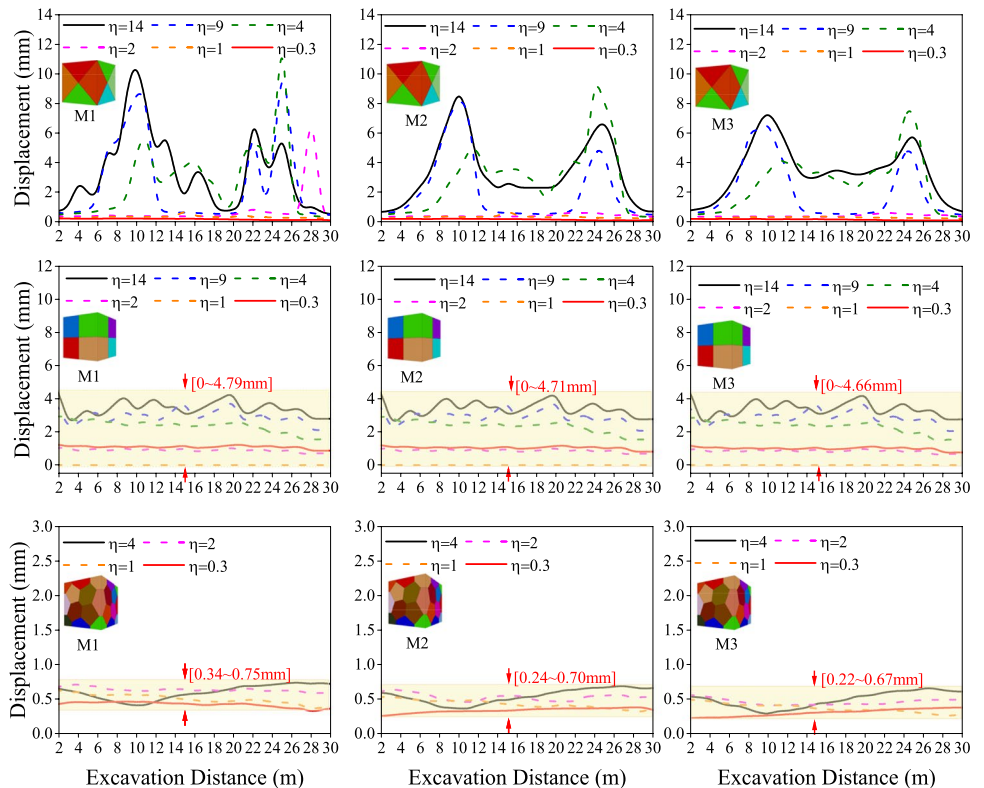
**Fig. 6** Vertical displacement of the surrounding rock at different sections of the tunnel (cubic blocks)



of  $\eta$ . It demonstrates that a higher degree of the fractured rock will form a wider disturbance region in the process of tunnel excavation and it is more likely to cause the uneven settlement of the deep surrounding rock. In fractured rock

with cubic blocks, the change interval of maximum displacement is mostly located at 0 to 4.79 mm when the value  $\eta$  varies from 0.3 to 14. When  $\eta$  is 0.3, 1, and 3, the maximum displacement along the direction of the tunnel is almost

**Fig. 7** Maximum displacement of surrounding rock with different sizes and shapes of blocks



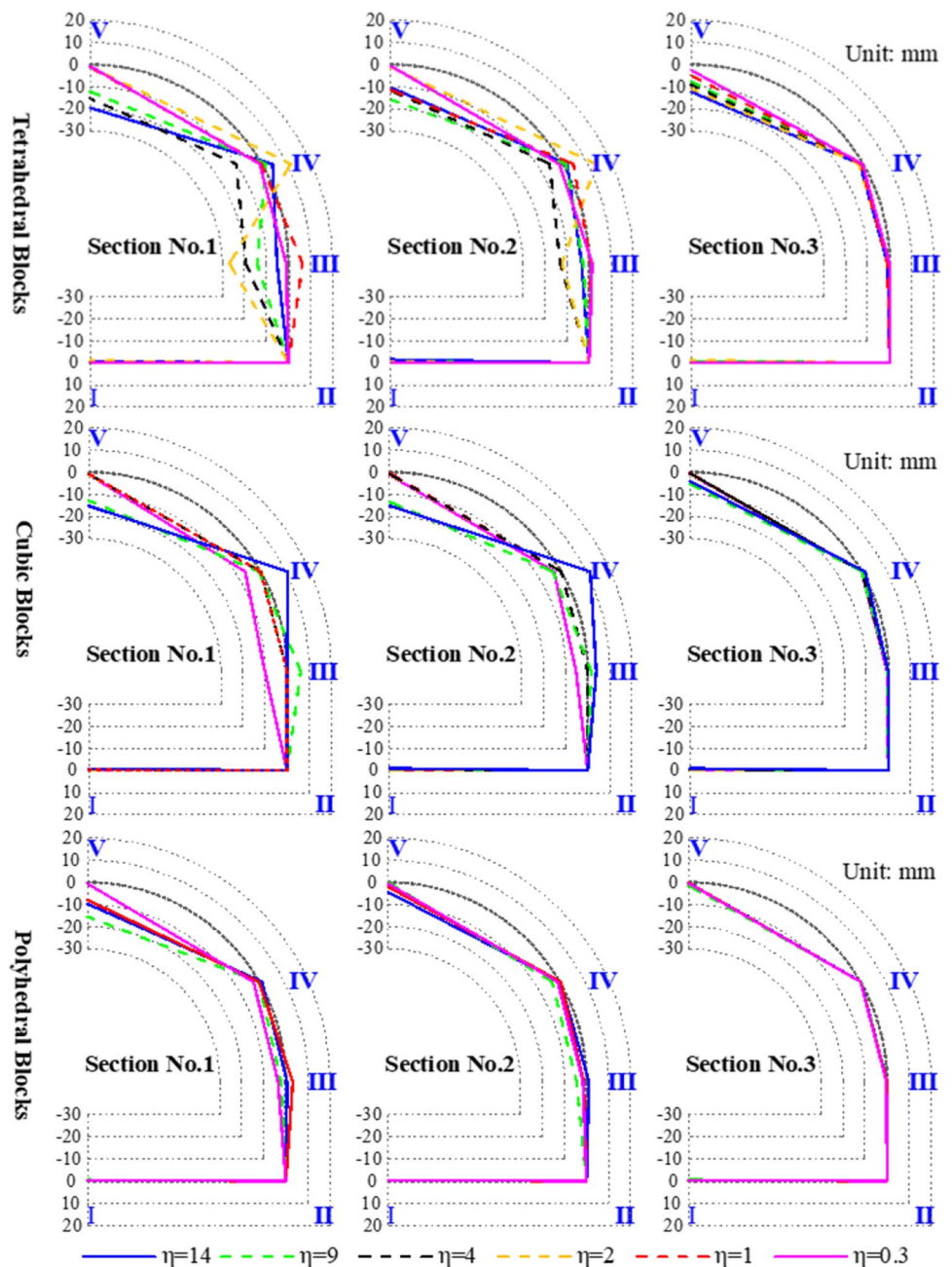
identical. In the fractured rock with polyhedral blocks, the change interval of maximum displacement is mostly located at 0.22 to 0.75 mm when the value  $\eta$  varies from 0.3 to 4. Therefore, these results strongly prove that characteristics of fractures have a great influence on tunnel excavation.

**Deformation characteristics of the tunnel**

Figure 8 illustrates the deformation characteristics of the tunnel built in the fractured rock with different sizes and shapes of blocks. It illustrates that the fractured rock composed of three types of blocks with different shapes

has similar effects on the deformation characteristics of the tunnel structure; i.e., the deformation value of the tunnel section far from the tunnel face (Section No. 1) is greater than that far from the tunnel face (Section No. 2 and Section No. 3), which is in agreement with the results of field testing. Meanwhile, with the increase of  $\eta$ , the deformation value relatively increases especially at the positions of III, IV, and V. The deformation of Section No. 1 is sensible to the change of  $\eta$  compared with the other two sections. Tunneling in the fractured rock with tetrahedral blocks has relatively larger deformation than other two shapes of blocks in the fractured rock.

**Fig. 8** Deformation characteristics of the tunnel built in the fractured rock with different sizes and shapes of blocks





The change of the  $\eta$  and the progress of excavation have little difference in the deformation at positions I and II, as their deformation value is small. In the fractured rock with tetrahedral blocks, for Section No. 1 and No. 2, positions III, IV, and V show relatively high values of deformation, and position V mainly perform the vertical settlement, and positions III and IV have both directions of deformation (expanding and closing) with the increase of  $\eta$  (larger  $\eta$  relatively shows larger deformation). But for Section No. 3, only the position of V has obvious deformation. The deformation characteristics of the tunnel in the fractured rock with cubic and polyhedral blocks are similar under the influence of the value of  $\eta$  and the tunnel depth, but with a smaller value.

Meanwhile, the vault settlement mainly dominates the tunnel deformation especially the fractured rock with tetrahedral blocks as it might generate greater uneven stress distribution, and their fractures easily propagate in the fractured rock than the other two shapes of blocks after excavation. Therefore, the process of tunnel excavation should focus on monitoring the tunnel vault deformation value. Timely taking effective measures in case of a large deformation value or deformation rate.

#### Maximum and minimum moment of tunnel liner

Figure 9 is the maximum and minimum moment of the tunnel liner built in the fractured rock with different shapes and sizes of blocks. It illustrates that the fractured rock composed of three types of blocks with different shapes has similar effects on the positive and negative moments of the liner. In the fractured rock mass formed by the same shape of blocks, the positive and negative moment values of the liner increase gradually with the increase of  $\eta$ . However, for different shapes of blocks, there are some differences concerning the increasing trend of the moment of the liner. For example, in the fractured rock with tetrahedral blocks, with the increase of  $\eta$ , the positive and negative moment values of liner show obvious non-linear characteristics, especially within the lower value of  $\eta$ . But in the fractured rock with cubic and polyhedral blocks, the increasing trend of the moment of the liner shows approximately linear. Meanwhile, for the same value of  $\eta$ , both the values of the positive and negative moment of the liner in the fractured rock with tetrahedral blocks are relatively larger than those in the fractured rock with cubic and polyhedral blocks.

To explain the relationship between the value of the moment and  $\eta$ , the major reason is that the geo-stress of the surrounding rock will redistribute after tunneling. The tetrahedral blocks might generate greater uneven stress distribution, and their fractures easily develop in the fractured rock than other two shapes of blocks after excavation. The propagation of small cracks in the fractured rock leads to the loss of the self-sustaining ability of the surrounding rock and

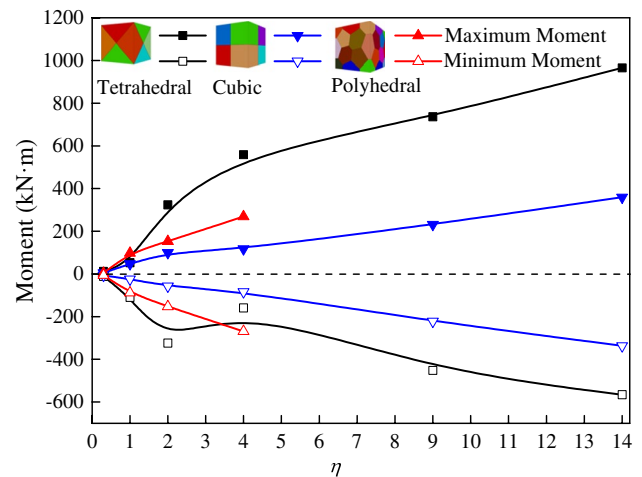


**Fig. 9** Maximum and minimum moment of the tunnel liner built in the fractured rock with different sizes and shapes of blocks

transfers loadings to the lining structure; the liner then has larger stress and moment. Hence, among three shapes of blocks, the tetrahedral blocks might generate larger positive and negative moment values in the tunnel liner. Therefore, considering the engineering practice, attention should be paid to the flexural and shear design of the tunnel lining structure to improve the safety of the tunnel excavation in fractured rock.

#### Conclusion

Based on a certain construction project, the surrounding rock displacement of the constructing tunnel was recorded by the field testing method, and the field testing results were verified by the numerical simulation. Besides, the impacts of different sizes and shapes of blocks in fractured rock have been further investigated through the numerical method. The following major conclusions can be drawn based on the results:

- (1) During the progress of tunnel excavation, the displacement of surrounding rock undergoes two major phases, i.e., the rapid growth phase and the gradual stabilization phase. The time interval of these two stages is different due to the different depths of the tunnel and the monitoring point.
- (2) In the same monitoring section, the closer to the vault of the tunnel, the larger the vertical displacement of the monitoring point. The displacement value of the section closer to the tunnel face is relatively larger than that far away from the tunnel face, as the vertical displacement of surrounding rock near the tunnel face is also affected by the backside excavated zone. The

larger length of the excavated zone is, the greater the influence on the vertical displacement of surrounding rock near the tunnel face will be. The tunnel section in shallower buried depth performs relatively larger liner deformation, and the vault of the tunnel has a larger deformation value compared with other positions on the tunnel section.

- (3) For the identical value of  $\eta$ , jointed rock masses formed by tetrahedral blocks perform relatively larger vertical displacement of surrounding rock, deformation of the tunnel, and positive and negative moments of liner structures than those formed by cubic or polyhedral blocks.

**Acknowledgements** All supports are gratefully acknowledged.

**Funding** This research was supported by National Natural Science Foundation of China (Grant No. 52038008 and 42107216), the Independent Scientific Research Project of Zhejiang Scientific Research Institute of Transport (Grant No. ZK202104 and No. ZK202105), Key Science and Technology Project of Transport Industry of Ministry of Transport (2021-MS2-061), the Project of Science and Technology Program of Department of Transport, Zhejiang Province (2021014), and Key Research and Development Plan Project of Zhejiang Province (2021C01106).

## Declarations

**Conflict of interest** The authors declare no competing interests.

## References

- Cacciari PP, Futai MM (2017) Modeling a shallow rock tunnel using terrestrial laser scanning and discrete fracture networks. *Rock Mech Rock Eng* 50(5):1217–1242. <https://doi.org/10.1007/s00603-017-1166-6>
- Do TN, Wu J-H (2020) Simulation of the inclined jointed rock mass behaviors in a mountain tunnel excavation using DDA. *Comput Geotech* 117:103249. <https://doi.org/10.1016/j.compgeo.2019.103249>
- Fan H, Li L, Liu H, Shi S, Hu J, Zhou S (2021) Advanced stability analysis of the tunnels in jointed rock mass based on TSP and DEM. *KSCE J Civ Eng* 25(4):1491–1503. <https://doi.org/10.1007/s12205-021-0170-2>
- Gao D, Zhang LQ, Rong HR, Bai-Lin MU, Wang DL (2017) Study on the plastic zone of the surrounding rock of jointed rock tunnel. *J Heb Instit Archit Civil Eng* (in Chinese). [http://en.cnki.com.cn/Article\\_en/CJFDTOTAL-HBJZ201701005.htm](http://en.cnki.com.cn/Article_en/CJFDTOTAL-HBJZ201701005.htm)
- Han D, Li K, Meng J (2020) Evolution of nonlinear elasticity and crack damage of rock joint under cyclic tension. *Int J Rock Mech Min Sci* 128:104286. <https://doi.org/10.1016/j.ijrmm.2020.104286>
- He S, Li Y, Aydin A (2018) A comparative study of UDEC simulations of an unsupported rock tunnel. *Tunn Undergr Space Technol* 72:242–249. <https://doi.org/10.1016/j.tust.2017.11.031>
- Itasca Consulting Group, Inc. (2020). *3DEC-3D distinct element code, Version 7.0, User's Manual*.
- Jia P, Tang CA (2008) Numerical study on failure mechanism of tunnel in jointed rock mass. *Tunn Undergr Space Technol* 23(5):500–507. <https://doi.org/10.1016/j.tust.2007.09.001>
- Jiang M, Liao Y, Wang H, Sun Y (2018) Distinct element method analysis of jointed rock fragmentation induced by TBM cutting. *Eur J Environ Civ Eng* 22(sup1):s79–s98. <https://doi.org/10.1080/19648189.2017.1385540>
- Jiang Q, Yang B, Yan F, Liu C, Shi Y, Li L (2020) New method for characterizing the shear damage of natural rock joint based on 3D engraving and 3D scanning. *Int J Geomech* 20:06019022. [https://doi.org/10.1061/\(ASCE\)GM.1943-5622.0001575](https://doi.org/10.1061/(ASCE)GM.1943-5622.0001575)
- Khan IA, Venkatesh K, Srivastava RK (2021) Elasto-plastic finite element analysis of twin tunnels — a comparison of excavation in intact and jointed rock mass. *Mater Today Proc*. <https://doi.org/10.1016/j.matpr.2021.05.122>
- Lei Q, Latham J-P, Xiang J, Tsang C-F (2017) Role of natural fractures in damage evolution around tunnel excavation in fractured rocks. *Eng Geol* 231:100–113. <https://doi.org/10.1016/j.enggeo.2017.10.013>
- Li Y, Qi T, Lei B, Qian W, Li Z (2019a) Deformation patterns and surface settlement trough in stratified jointed rock in tunnel excavation. *KSCE J Civ Eng* 23(7):3188–3199. <https://doi.org/10.1007/s12205-019-0477-4>
- Li ZL, Li JC, Li X (2019b) Seismic interaction between a semi-cylindrical hill and a nearby underground cavity under plane SH waves. *Geomech Geophys Geo-Energy Geo-Resour* 5(4):405–423. <https://doi.org/10.1007/s40948-019-00120-5>
- Pan C, Li X, Li J, Zhao J (2021) Numerical investigation of blast-induced fractures in granite: Insights from a hybrid LS-DYNA and UDEC grain-based discrete element method. *Geomech Geophys Geo-Energy Geo-Resour* 7(2):49. <https://doi.org/10.1007/s40948-021-00253-6>
- Panthee S, Singh PK, Kainthola A, Singh TN (2016) Control of rock joint parameters on deformation of tunnel opening. *J Rock Mech Geotech Eng* 8(4):489–498. <https://doi.org/10.1016/j.jrmge.2016.03.003>
- Qu T, Wang Z, Zhao W, Pan K (2021) Research on meso-mechanism of failure mode of tunnel in jointed rock mass. *Geotech Geol Eng* 1–11. <https://doi.org/10.1007/s10706-021-01761-8>
- Shi Q, Mishra B (2021) Discrete element modeling of delamination in laboratory scale laminated rock. *Mining, Metallurgy & Exploration* 38(1):433–446
- Shi Q, Mishra B, & Zhao Y (2022) DEM analysis of the effect of lamination properties on the stability of an underground coal mine entry with laminated shale roof. *Mining, Metallurgy & Exploration*, 1–12.
- Singh M, Rao KS, Ramamurthy T (2002) Strength and deformational behaviour of a jointed rock mass. *Rock Mech Rock Eng* 35(1):45–64
- Wang X, Cai M (2020) A DFN–DEM multi-scale modeling approach for simulating tunnel excavation response in jointed rock masses. *Rock Mech Rock Eng* 53(3):1053–1077. <https://doi.org/10.1007/s00603-019-01957-8>
- Wang X, Li J, Zhao X, Liang Y (2022) Propagation characteristics and prediction of blast-induced vibration on closely spaced rock tunnels. *Tunn Undergr Space Technol* 123:104416. <https://doi.org/10.1016/j.tust.2022.104416>
- Wang X, Yuan W, Yan Y, Zhang X (2020) Scale effect of mechanical properties of jointed rock mass: a numerical study based on particle flow code. *Geomech Eng* 21(3):259–268
- Wang Z, Gu L, Zhang Q, Jang B-A (2021) Influence of initial stress and deformation states on the shear creep behavior of rock discontinuities with different joint roughness coefficients. *Rock Mech Rock Eng* 54(11):5923–5936. <https://doi.org/10.1007/s00603-021-02633-6>

- Yang H, Duan HF, Zhu JB (2019a) Ultrasonic P-wave propagation through water-filled rock joint: an experimental investigation. *J Appl Geophys* 169:1–14. <https://doi.org/10.1016/j.jappgeo.2019.06.014>
- Yang R, Ding C, Yang L, Chen C (2018) Model experiment on dynamic behavior of jointed rock mass under blasting at high-stress conditions. *Tunn Undergr Space Technol* 74:145–152. <https://doi.org/10.1016/j.tust.2018.01.017>
- Yang W, Zhang Q, Ranjith PG, Yu R, Luo G, Huang C, Wang G (2019b) A damage mechanical model applied to analysis of mechanical properties of jointed rock masses. *Tunn Undergr Space Technol* 84:113–128. <https://doi.org/10.1016/j.tust.2018.11.004>
- Zhang R, Chen G, Zou J, Zhao L, Jiang C (2019) Study on roof collapse of deep circular cavities in jointed rock masses using adaptive finite element limit analysis. *Comput Geotech* 111:42–55. <https://doi.org/10.1016/j.compgeo.2019.03.003>
- Zhang W, Xu B, Mei J, Yue G, Shi W (2020) A numerical study on mechanical behavior of jointed rock masses after tunnel excavation. *Arab J Geosci* 13(11):416. <https://doi.org/10.1007/s12517-020-05358-y>
- Zhou C, Xu C, Karakus M, Shen J (2019) A particle mechanics approach for the dynamic strength model of the jointed rock mass considering the joint orientation. *Int J Numer Anal Meth Geomech* 43(18):2797–2815. <https://doi.org/10.1002/nag.3002>